# Evaluation and Reduction of Elevated Height Printing Defects

***Dan Barnett and Marlene McDonald; Fujifilm Dimatix; Lebanon, NH/USA***

## Abstract

*Ink jet printing at elevated heights is known to initiate unsteady laminar flows which lead to imaging defects often referred to as wood-grain or fogging. An investigation of the unsteady flow development was conducted using both experimental and numerical simulation techniques. High speed imaging revealed that the interaction between the air flow induced from droplet drag and the couette flow entrained from the substrate motion develops large eddies which roll along the droplet stream and lead to unsteady flows causing wood-grain defects. ANSYS CFX computational fluid dynamics (CFD) simulations are presented to support the experimental results and to provide a higher degree of understanding of the flow dynamics. Several techniques are revealed which illustrate how wood-grain defects can be improved. These techniques strive to enable ink jet technologies to be used in a wider range of applications with large height variations or which require jetting at elevated heights to prevent contact with print heads.*

*In addition to unsteady flow defects, two other phenomenons related to elevated height printing were included in this study: (1) excessive nozzle plate wetting and (2) excessive drag on droplets ejected into a still flow field.*

## Nomenclature

| | |
|---|---|
| $a$ | Instantaneous acceleration |
| $A$ | Cross-sectional area of the drop sphere |
| $\rho$ | Density of jetting environment (1.20 kg/m$^3$ for air at 20°C) |
| $C_D$ | Drag coefficient |
| $F_D$ | Drag force |
| $d$ | Drop diameter |
| $h$ | Height of nozzle plate from substrate |
| $L$ | Characteristic length for Reynolds Number.<br>Flow past drops: L = drop ∅. Couette flow: L = gap height. |
| $m$ | Drop mass |
| $Re$ | Reynolds number |
| $V$ | Velocity |
| $\mu$ | Viscosity of jetting environment (1.80e-5 N*s/m$^2$ for air at 20°C) |

## Introduction

The inkjet printing industry is striving to pursue new, elevated height printing applications and applications with large height variation in a variety of markets. In order to successfully implement printing processes at elevated printing heights, a fundamental understanding of the influence of air flow on printing defects must be achieved. The flow profile under inkjet print heads is influenced by two independent sources: (1) couette flow is entrained under the print head by a relative velocity difference between the print head and the substrate and (2) air flows are entrained by jetting a stream of droplets (referred to as droplet jets herein). As indicated previously by Hsiao et al, wood-grain defects are initiated by unsteady flows which develop due to the interaction between the droplet jets and the couette flow at high printing heights.[1] While additional experiments have been conducted to determine the influence of the air flow on drop displacement, these earlier studies were conducted at normal printing heights (2 mm) which do not initiate unsteady flows.[2,3] Additionally, while measurements have been taken previously to determine if the droplet wakes significantly interact with the couette flow, they were conducted on individual drops therefore the flow entrainment from the jetted drop was minimal and droplet jets did not develop.[2]

The study presented in this paper was initiated with the intent of determining the factors leading to unsteady flows and high height printing defects however expanded to include the evaluation of numerous solutions. To further improve the understanding of how the flow dynamics change under different conditions, computational fluid dynamics (CFD) was utilized with particle tracking to simulate the interaction between the couette flow and the droplet jets. Experiments were then conducted to evaluate various hypotheses of how high height printing defects could be significantly improved.

## Printed Image Experiments

Evaluation of the leading factors influencing wood-grain defects began by printing hundreds of images on a sled printer. An image pattern of 256 lines spaced at 100 dpi (cross process) x 400 dpi (process direction) and 2400 pixels long (6") was used. The images were displayed as height versus printing frequency / speed 'storyboards' which were used to qualitatively determine the severity of wood-graining under the various test conditions. A linear motor sled printer was chosen for these experiments due to the precision and repeatability of the motion and height control. Additionally, results were validated on a web drive printer to ensure that air flow effects due to the sled motion do not alter the behavior of the unsteady flow under the print head. The images were printed using a black ceramic ink on a 10 mil photo base substrate. The primary objective of these tests was to evaluate the effect of nozzle spacing on wood-grain defects. The majority of the tests utilized 100 dpi native resolution print heads with the nozzles arranged in either 1 or 2 rows (*figs. 1 & 2*).

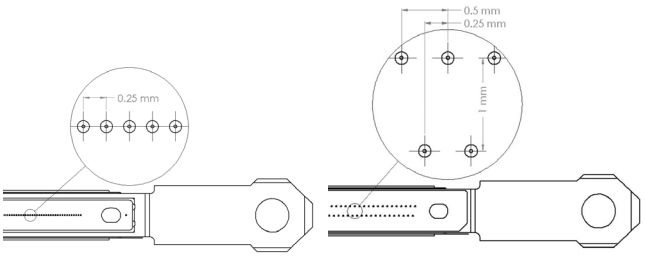


***Figures 1 & 2.*** *Single row at 100 nozzles per inch (left) / Dual row at 50 nozzles per inch (right)*

Primary test variables include:

- X-Process Nozzle Spacing: 0.25 mm & 0.5 mm
- X-Process Print Resolutions: 100, 200 & 400 dpi
- Process Print Resolution: 400 dpi
- Standoff: 2.5 mm, 3.8 mm & 5.1 mm
- Drop Ejection Velocity: 7 m/s time of flight
- Frequency: 4 – 24 kHz
- Substrate Velocities: 0.25 – 1.51 m/s (frequency dependent)
- Drop Mass: 33-43 ng (native) & 95-110 ng (multi-pulse)

The time of flight drop velocity was measured by the time differential between the drop actuation and when the droplet reaches 0.76 mm. The drive voltage required to jet at 7m/s was then determined for each print head tested and the drop mass was recorded. This normalized drop mass was used throughout the tests to ensure that the various print heads were all jetting at 7m/s.

## Printed Image Results & Observations

As observed throughout this study, wood-grain defects are either caused by patterns of satellite or main drop placement errors. Whether the defects observed by the human eye are caused by satellite or main drops are primarily attributed to both the main drop placement errors and the nominal non-printed distance between drops. For example, satellite drop wood-graining was more visible when printing lines at 100 lines per inch; however main drop wood graining became visibly dominant at 200 or more lines per inch (*fig. 3*).

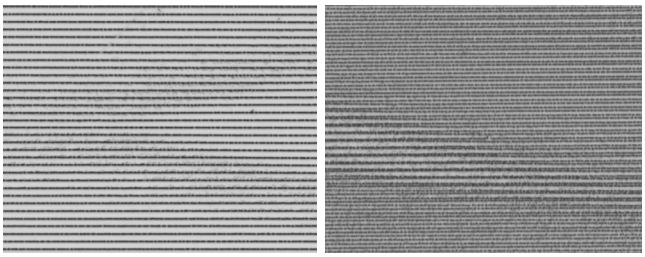

***Figure 3.*** *Magnification of wood-grain visible from satellite drop errors at 100 lines per inch (left) and main drop errors at 200 lines per inch (right).*

To study the effect of nozzle spacing on wood-grain defects, print heads configured with nozzles in two rows were compared to print heads with nozzles in a single row at the same native resolution. The images in figure 4 emphasize the effect of nozzle spacing on wood-grain defects. These images were printed at a height of 5.1 mm (nozzle plate to substrate) using jetting frequency and substrate speed combinations to maintain a process resolution of 400 dpi. Wood-grain defects were observed to occur consistently at a standoff of 3.8 mm with the 100 npi print heads. When the height was reduced to 3.5 mm, only occasional minor wood-grain defects were observed.

These results show that the wood-grain defects are highly dependent on the interaction between the couette and droplet flows. Increasing the nozzle spacing reduces the resistance on the couette flow as it flows past the droplet curtain. The lower flow resistance reduces the flow interactions which lead to unsteady flows and wood-grain defects.

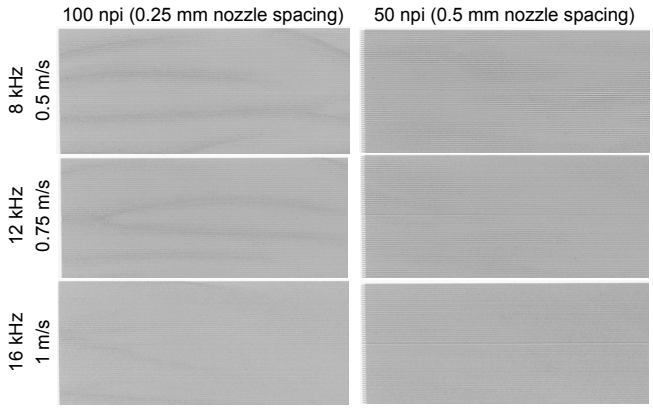


***Figure 4.*** *Nozzle spacing comparison @ 5.1 mm. Leading edge is visible at the right by the wood-grain development region.*

Interestingly, when the printing speed was increased to 16 kHz and 1m/s, the visibility of wood-graining was observed to decrease (*fig. 4)*. The reduction in wood-grain defects was suspected to have been attributed to both the increased couette flow entrained by the faster substrate speed motion and reduction of droplet drag due to the increasing slipstream at higher frequencies. Two experiments were performed to validate these hypotheses: (1) inducing forced air upstream of the print head in the direction of substrate motion and (2) conducting experiments to measure the droplet drag at different frequencies.

To evaluate the effect of increasing the flow rate under the print head, a plenum was manufactured using a FDM printer. The device consisted of an upper chamber where gas is supplied via three ports, a layer of filters to provide a uniform velocity flow field and an outlet duct. The plenum was positioned upstream of the print head to assist additional flow under the print head using entrainment from the moving substrate (*fig. 5)*. The gas supply was precisely controlled using a mass flow controller.

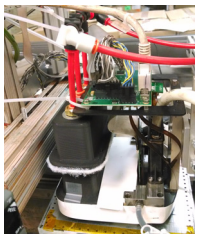

***Figure 5.*** *Set-up for forced gas test.*

***Figure 6.*** *Set-up for air baffle test.*

As the mass flow rate of air was increased, the severity of the wood-grain decreased; however fogging began to appear at high flow rates (80 lpm) before the wood-grain patterns were completely eliminated (*fig. 7*). Note that the flow rates reported here are intended as a relative comparison since only a fraction flowed under the print head.

Another hypothesis evaluated was that reducing the density of the jetting environment would reduce unsteady flows. From fluid dynamics, we know that the droplet drag is proportional to the fluid properties of the jetting environment (*eq. 1 & 2*). Therefore, it was suspected that a lower density gas would reduce the Reynolds number, and also the flow entrained by the droplet jetting, thereby reducing the unsteady flows. [4]

$$C_D = \frac{F_d}{\frac{1}{2}\rho v^2 A} \quad (1)$$

$$\mathrm{Re} = \frac{\rho \cdot V \cdot L}{\mu} \quad (2)$$

This theory was evaluated by repeating the forced air test with forced helium. The lower density and similar viscosity of helium compared to air resulted in a reduction of the Reynolds number by a factor of 7.1.[4] The results from these tests concluded that jetting into a low density gas jetting environment was highly successful at eliminating wood-grain defects (*fig. 7*).

It should be noted that the helium flow rates tested were orders of magnitude greater than what would be required if implemented into an industrial printing system. The majority of the helium flow, for example, could be greatly reduced if intelligent machine design practices were used to recycle the helium gas within a chamber around the printing area. Due to the high cost of helium gas, this would be critical to incorporate this technology into an economically viable printing solution.

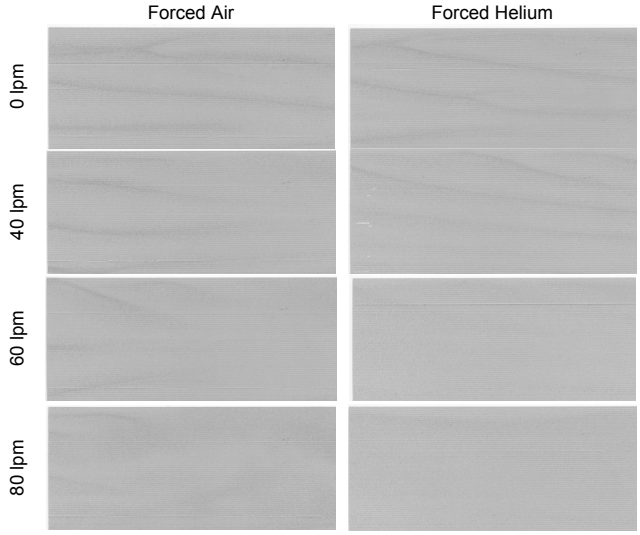


***Figure 7.*** *Forced Air & Helium Results, 100 npi, 5.1 mm, 8 kHz & 0.5 m/s.*

In another experiment, entrance and exit geometry were evaluated by constructing 1" wide baffles which were coplanar to the nozzle plate (*fig. 6*). These crude modifications did not eliminate the wood-graining at 100 npi, a height of 3.8 mm and 8 kHz however they do illustrate how geometry can help to streamline the flow under the print head. Some improvement was observed when either the inlet or exit baffles were implemented and the greatest improvement was observed when both were used simultaneously (*fig. 8*).

Although wood-grain was not eliminated during these tests, they illustrate how it is important to consider the effects of the surrounding geometry on the flow under print heads. New elevated height printing systems should be designed to reduce disturbances to the flow under the print heads.

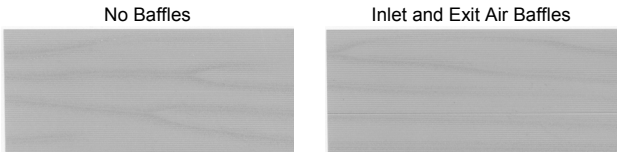


***Figure 8.*** *Entrance and exit geometry modification results.*

## High Speed Imaging Observations

High speed imaging was utilized to analyze the development of the unsteady flows that initiate wood-grain. A Photron SA5 high speed camera was used for these experiments with the drops illuminated with backlighting. Flow visualization was achieved by using a nebulizer to seed the couette flow with approximately ∅1-5 micron drops of de-ionized water (*fig.9*). As a separate test, the camera was repositioned at a viewing angle normal to the print head to capture the path of the drops during flight as wood-grain development occurs (*fig. 10*).

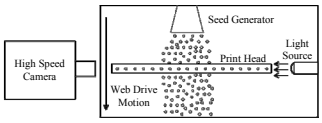


***Figure 9.*** *Visualization of flow under print head during jetting.*

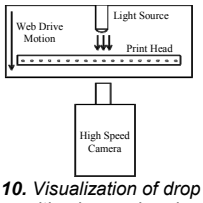


***Figure 10.*** *Visualization of drop motion resulting in wood-grain defects.*

Visualization of the flows under the print head was done using conditions which were previously determined to result in severe wood-grain defects. A row of nozzles spaced at 100 npi were set to eject drops simultaneously at 7m/s and 8kHz. The print head height and substrate speed were set to 5mm and 0.5m/s respectively. Using particle tracking techniques, the interaction of the air flows were observed. As the air flow which developed from the droplet drag impinged on the substrate, it abruptly changed direction to flow normal to the droplet curtain and parallel to the substrate. On the upstream side of the droplet curtain and near the substrate, the droplet drag flow opposed the substrate entrained couette flow and a large eddy developed (*fig. 11*). This eddy is of significance because it enables high velocity flows to interact with the drops for greater than half of their flight time and can lead to significant drop placement errors.

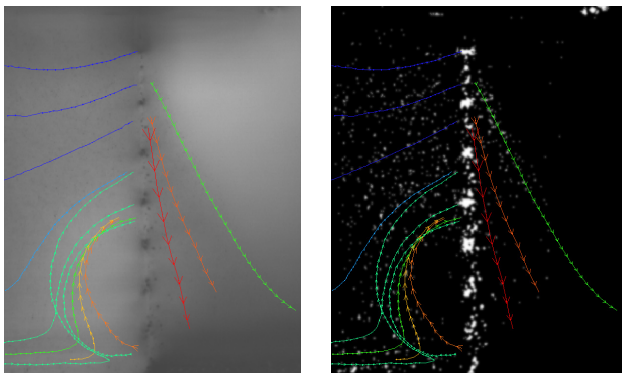

***Figure 11.*** *Particle tracking from high speed video. Raw image (left), filtered (right). Colors indicate max velocity: bl=.5-.75 m/s, lt bl=.75-1.0, lt gr = 1-1.25, gr=1.25-1.5, yel=1.5-1.75, lt or=1.75-2, or=2-2.5, drk or=2.5-3, red=4.5.*

Figure 12 shows the path of satellite drops as they begin to develop a satellite wood-grain defect on the substrate as viewed normal to the row of nozzles. The satellites on the right side of the image are aligned with the main drops while the satellites on the left side are displaced by a cross flow causing the satellites to fill the areas intending to be non-printed. Subsequent frames of the high speed video show the satellite displacement moving left to right and periodically repeating as is also observed in the printed wood-grain images. The frequency of oscillation from the high speed video analysis was measured to be 5-10 Hz. The frequency of oscillation can alternatively be determined by measuring the distance between wood-grain defects along the process direction. Although not extensively tested as part of this study, the frequency of oscillation can be used as an indicator to evaluate new wood-grain reduction techniques.

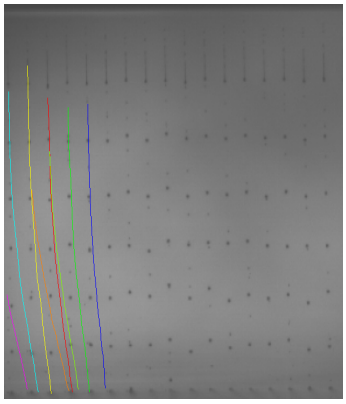

***Figure 12.*** *Particle tracking of satellite drops as viewed normal to nozzle row to visualize and quantify cross-process placement errors.*

## Numerical Evaluation of Unsteady Flows

An improved understanding of how jetting conditions affect the flow under the print head has been achieved using ANSYS CFX. The simulations were modeled as a half symmetry model of a 256 jet stationary print head with the substrate moving at 0.5m/s. The droplet jets developed by the droplet streams were simulated using a particle tracking model to simulate ejection of 40 ng drops at a 7m/s and 8kHz over a 5mm gap.

### *Mesh Geometry*

An efficient mesh was generated by sub-dividing the fluid region into multiple rectangular bodies and meshed with a combination of ANSYS multi-zone and hex dominant meshing methods. The mesh was refined to a size of 50 microns in the region surrounding the droplet paths and gradually increased to 2mm. The resulting mesh yielded 2.6M nodes and 3.0M elements (*fig. 13*).

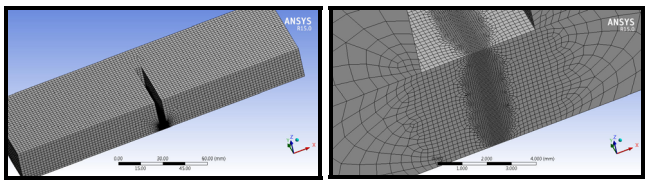

***Figure 13.*** *Mesh used for CFD simulations.*

### *Boundary Conditions & Solution Strategy*

Prior to introducing particle tracking, the model was first solved as a steady state analysis to develop the couette flow under the print head (*fig. 14*). To be able to directly compare to the high speed video experiments presented earlier in this paper, the substrate was simulated as a wall moving at 0.5m/s. Stationary walls were applied to the print head surfaces and non-wall surfaces were modeled as openings at 1 atm. The Reynolds number computed at the simulated conditions of 5mm and 0.5m/s in air at 20°C was 167 which is significantly below the onset of turbulence (~2000), therefore a laminar flow model was applied.[4]

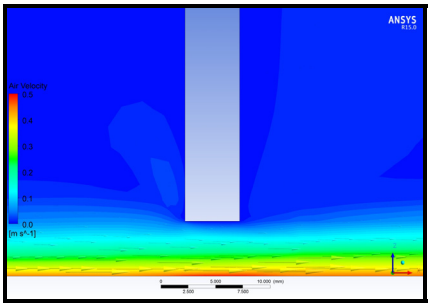

***Figure 14.*** *Couette flow result used as an initial condition for transient runs.*

After convergence of the couette flow solution particle injections were added at each nozzle location and set to eject ∅42 micron and 40ng drops at a rate of 7m/s and 8kHz. The substrate surface was configured to absorb all particles to prevent them from bouncing off of the wall and causing additional disturbances to the flow. Since the flow had been determined to be in the laminar flow regime both experimentally and theoretically, the Schiller-Naumann drag model was applied to the particles.[5]

$$C_D = \frac{24(1 + 0.15\,\mathrm{Re}^{.687})}{\mathrm{Re}} \qquad (3)$$

The transient simulation was solved for a total time duration of 100ms using time steps of $1e^{-5}$ s. This time step was used to ensure that there were sufficient time steps between subsequent drops and small enough for the mesh size to velocity ratio.

### *Transient Results*

Similar to the experimental results, simulated results showed that the eddy became fully developed in approximately 50 ms (*fig. 15*). The motion of the eddy along the droplet curtain was visualized by creating a cross section through the eddy at 3mm below the print head (*fig. 16-17*). As the eddy started to roll along the length of the droplet curtain, cross flows occurred and exerted forces on the drops in the cross process direction. These external forces are the root cause of drop placement errors and wood-grain imaging defects.

In addition to comparing the eddy development time, these simulation results were validated by comparing velocities in the eddy to the experimental results. The simulated droplet drag was also verified by comparing the reduction of drop velocity during flight from the experimental and simulated results. These comparisons concluded that these techniques closely approximate the interaction of the flows under the print head and are useful for the development of new print heads.

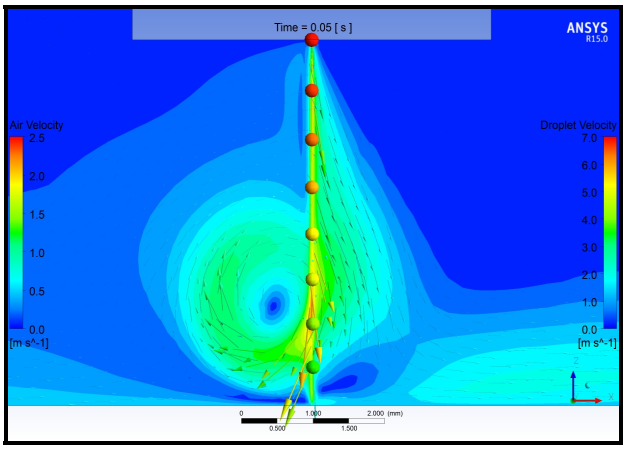


***Figure 15.*** *Upstream eddy observed using CFD @ t=50ms. Substrate moving left to right. Drop size enlarged for visualization.*

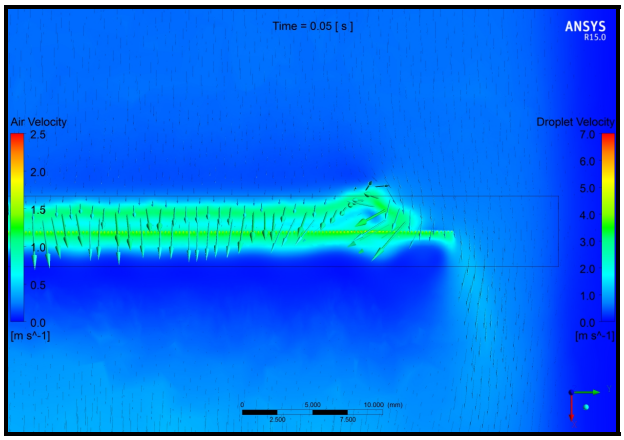


***Figure 16.*** *CFD results 3mm below the print head @ t=50ms.*

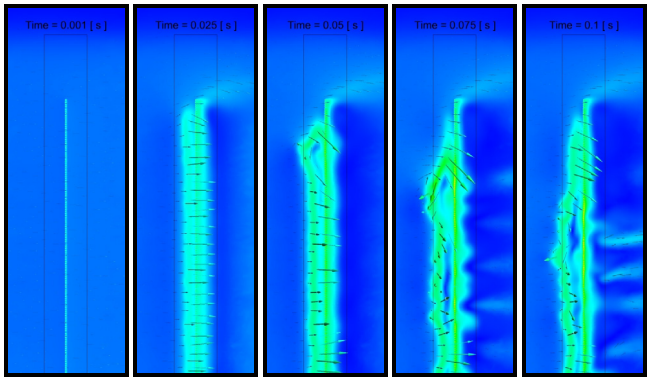


***Figure 17.*** *Transient response of flow 3mm under the print head.*

## Droplet Drag Considerations

Droplet drag requires careful consideration specifically when jetting small drops from high heights. The primary concern is that smaller drops are ejected with a low initial momentum due to their low mass and they more rapidly decrease in velocity during flight. As the velocity decreases, additional momentum is lost which enables the drops to more easily be displaced by the air flow forces which are present below the print head. The reduction in velocity during flight can be approximated by using the drag coefficient shown previously in *eq. 3* to calculate the drag force during flight:[4]

$$F_D = \frac{1}{2} \cdot \rho \cdot V^2 \cdot C_D \cdot A \tag{4}$$

The force of gravity can be considered negligible and from Newton's 2nd Law the deceleration rate is simplified as:

$$a = \frac{F_D}{m} = \frac{\frac{1}{2} \cdot \rho \cdot V^2 \cdot C_D \cdot A}{m} \tag{5}$$

The graph shown in figure 18 demonstrates how the velocity of drops with mass less than 10 ng rapidly decrease during flight. This graph was computed using drag coefficients reduced by 15% to account for the reduction of drag due to the slipstream which develops when jetting subsequent drops. A drag reduction of 15% was determined experimentally with the high speed camera by monitoring the reduction of velocity during flight for 5-10 ng drops.

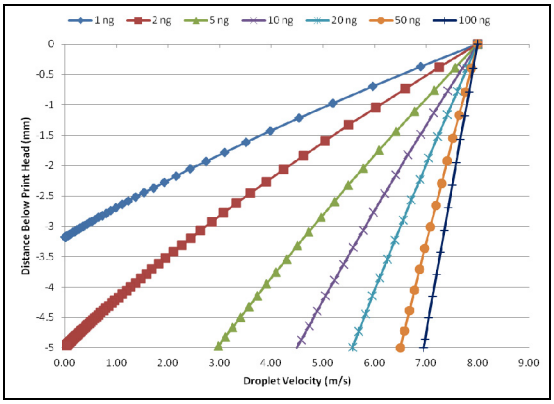


***Figure 18.*** *Calculated reduction in drop velocity for 1-100 ng drops.*

An additional consideration of droplet drag at high printing heights is the transient response when jetting small drops into a still flow field. There is more drag force exerted against the first few drops before the slipstream is developed and the deceleration induced by the drag force can lead to a significant reduction in velocity during flight. This was evaluated by measuring the total flight time for the first 50 drops ejected from a nozzle as they travel across a 5 mm gap for different drop masses and ejection velocities.

As observed during these tests, certain conditions can cause the flight time of the first drops ejected to be nearly 50% longer than the steady state flight time (*fig. 19*). An interesting observation is achieved by comparing the 6.1 ng drops ejected at 6.6 m/s to 10.7 ng drops ejected at 8.0 m/s. The smaller and slower drops took longer to reach steady state due to the low final velocity at the substrate (2.5 m/s) while the larger drops reach steady state faster due to the greater momentum and smaller decrease in velocity. Since steady state was reached within the first 20 drops, it is unlikely that this would lead to significant imaging defects however this should be considered when viewing leading

edge defects. Additional experiments were also conducted at 20 and 40 kHz and yielded very similar results to the 10 kHz results presented.

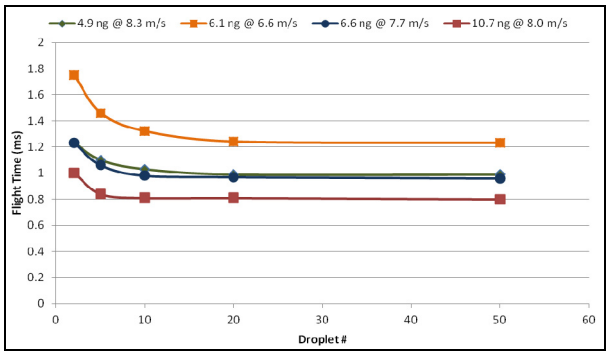


***Figure 19.*** *Effect of small drops jetting into a still flow field. Height = 5mm.*

## Nozzle Plate Wetting

In some applications, nozzle plate wetting has been observed to cause drops to be ejected with large trajectory errors or to prevent nozzles from ejecting drops altogether. While wood-grain defects are the leading elevated height defect for drop masses larger than 20 ng, excessive nozzle plate wetting has been observed to be a significant problem for jetting drops smaller than 10 ng. This is more commonly observed to be problematic for applications jetting smaller drops because the satellite drops can be small fractions of a nanogram. These micro satellites rapidly lose velocity in the first couple millimeters of flight and are then easily captured into eddies previously discussed and re-deposited on the nozzle plate. Since the satellites require very small forces to move them, air flow can be introduced to blow them away from the nozzle plate without causing placement errors on the main drops. In this manner, it has been shown that forced air can be used to simultaneously reduce nozzle plate wetting as well as wood-grain defects.

## Conclusions

As a result of this study, a fundamental understanding of the development of unsteady flows leading to wood-grain defects has been achieved. Wood-grain defects are now understood to be initiated by the interaction of the flow entrained due to droplet drag and the couette flow entrained by the motion of the substrate or print head. This interaction of flows has been observed to develop into large unsteady eddies which roll along the droplet curtain and initiate cross flows exerting forces on the drops leading to wood-grain defects.

Several techniques have been demonstrated to significantly reduce wood-grain defects and to enable printing applications at higher heights:

- Air flow control via eddy stabilization
- Reduce density of jetting environment leading to reduced drag and smaller eddies
- Increased spacing between nozzles
- Geometry modifications to stabilize flows
- Reduced satellite printing waveforms

In addition to using air flow to reduce wood-grain defects, it can simultaneously drastically improve print head sustainability by reducing the mean time between jetting failures. Specifically troublesome when jetting small drops at high heights, satellite drops can frequently re-deposit on the nozzle plate and interfere with jetting. Air flow has been observed to displace the satellite drops downstream past the printing area where they can be collected using a slight vacuum.

The experimental and numerical simulations techniques utilized throughout this study, specifically high speed imaging and computational fluid dynamics, have proven to be invaluable tools for obtaining a fundamental understanding of flow related printing defects. Future print head designs will be developed using these techniques to enable new print head products to be used in a wider rage of applications.

## References

[1] W.-K. Hsiao, G.D. Martin, S.D. Hoath, I.M. Hutchings, M. Hook and M. Massucci, Evidence of Print Gap Airflow Affecting Web Printing Quality, Proc. IS&T's NIP29: 29th Intl. Conf. on Digital Printing Technology, pg. 303-306. (2013).

[2] W.-K. Hsiao, S.D. Hoath, G.D. Martin, and I.M. Hutchings, Aerodynamic Effects in Ink-Jet Printing on a Moving Web, Proc. IS&T's NIP28: 28th Intl. Conf. on Digital Printing, pg. 412-415. (2012).

[3] Link, N., Lampert, S., Gurka, R., Liberzon, A., Hetsroni, G., and Semiat, R., "Ink drop motion in wide-format printers II. Airflow investigation," Chem. Eng. Process., 48, (2009) pg. 84-91.

[4] F. M. White, Fluid mechanics, 3rd ed. (McGraw-Hill, New York, NY, 1994) pg. 328-329, 387-424, 701-702.

[5] ANSYS CFX-Solver Theory Guide, Release 14.5. (ANSYS, Canonsburg, PA, 2012) pg. 154.

## Author Biography

*Dan Barnett received his BS degree in Mechanical Engineering from the University of Vermont in 1999 and is registered as a Professional Engineer. In September of 2013, Dan joined Dimatix as a development engineer. Prior to joining the ink jet industry he worked for 15 years as a development engineer in the injection molding and plasma cutting industries. Throughout his career he has utilized experimental and numerical techniques to develop unique solutions to challenging problems.*

*Marlene McDonald has worked as a development engineer at FUJIFILM Dimatix in Lebanon, NH since 1994. She has been focused on computational modeling, jet design, and new product development for many unique applications. Marlene received her BA in Engineering Sciences from Dartmouth College and her MSME in Fluid Mechanics from the University of Massachusetts at Amherst.*